American Mineralogist, Volume 96, pages 179–187, 2011

The crystal structure of stichtite, re-examination of barbertonite, and the nature of polytypism in MgCr hydrotalcites

Stuart J. Mills,[1,*] Pamela S. Whitfield,[2] Siobhan A. Wilson,[1,†] Joanne N. Woodhouse,[1,‡] Gregory M. Dipple,[1] Mati Raudsepp,[1] and Carl A. Francis[3]

[1]Mineral Deposit Research Unit, The University of British Columbia, Vancouver, British Columbia V6T 1Z4, Canada
[2]Institute for Chemical Process and Environmental Technology, National Research Council of Canada, Montréal Road, Ottawa, Ontario K1A 0R6, Canada
[3]Harvard Mineralogical Museum, 24 Oxford Street, Cambridge, Massachusetts 02138, U.S.A.

Abstract

Stichtite, ideally $Mg_6Cr_2CO_3(OH)_{16}\cdot 4H_2O$, from Stichtite Hill, Tasmania, Australia, and barbertonite, also ideally $Mg_6Cr_2CO_3(OH)_{16}\cdot 4H_2O$, from the Kaapsehoop asbestos mine, South Africa, have been studied by powder X-ray diffraction and their structures have been refined using the Rietveld method. Stichtite from Stichtite Hill crystallizes in the rhombohedral space group $R\bar{3}m$, with unit-cell parameters a = 3.09575(3) and c = 23.5069(6) Å, V = 195.099(6) Å^3, with Z = 3/8. Barbertonite from the Kaapsehoop asbestos mine crystallizes in the hexagonal space group $P6_3/mmc$. The co-type specimens of barbertonite were found to be intergrown mixtures consisting of barbertonite and stichtite. Unit-cell parameters of barbertonite from the co-type specimens were a = 3.09689(6), c = 15.6193(8) Å, and V = 129.731(8) Å^3 and a = 3.09646(6), c = 15.627(1) Å V = 129.76(1) Å^3, and Z = ¼. Rietveld refinements of both stichtite and barbertonite show that they are polytypes rather than polymorphs and do not represent distinct mineral species. Several possible nomenclature systems are discussed for the naming of hydrotalcite minerals and groups. Raman band assignments are also presented for stichtite from Stichtite Hill.

Stichtite and hydrotalcite minerals make up a large proportion of the ore at the Mount Keith nickel mine in Western Australia. Bulk powder diffraction shows the ore contains 6.1 wt% stichtite and 5.6 wt% iowaite. Hydrotalcite group minerals provide an important potential reservoir of CO_2. At Mount Keith, the amount of CO_2 mined as stichtite could exceed 45 000 metric tons per year, while exchange of Cl for CO_3 could fix in excess of 40 000 metric tons CO_2 per year if end-member iowaite is reacted to form pyaroaurite.

Keywords: Stichtite, barbertonite, polytype, hydrotalcite, carbon sequestration, Stichtite Hill, Kaapsehoop asbestos mine, X-ray diffraction

Introduction

Stichtite, ideally $Mg_6Cr_2CO_3(OH)_{16}\cdot 4H_2O$, is the Cr-analog of hydrotalcite, which occurs in Cr-bearing serpentinites, ophiolites, and greenstone belts in several localities worldwide. Originally identified as "kämmererite" [Cr-rich clinochlore – Nordenskiöld (1840); Lapham (1958)] in 1891, stitchtite was recognized as a non-silicate in 1910 (Petterd 1910) and was formally described in 1914 from Stichtite Hill (41°53′9″S, 145°26′16″E), Dundas, Tasmania, Australia (Twelvetrees 1914). It was named stichtite after Robert Sticht, general manager of the Mt. Lyell mines in Tasmania, and a world-renowned metallurgist. The most comprehensive work on the crystal chemistry and provenance of stichtite was done by Ashwal and Cairncross (1997), who summarize all previous data on stichtite. Bottrill and Graham (2006) provide further information on the Tasmanian occurrences of this mineral and Mondal and Baidya (1996) provide information on stichtite from the Nuasahi chromite deposits, eastern India.

Barbertonite, also ideally $Mg_6Cr_2CO_3(OH)_{16}\cdot 4H_2O$, was described by Frondel (1941) as the hexagonal polymorph of stitchtite from Kaapsehoop asbestos mine, Kaapsehoop, Barberton district, Mpumalanga, South Africa. Barbertonite was initially identified by X-ray diffraction films which showed a similarity to the diffraction patterns of sjögrenite [$Mg_6Fe_2CO_3(OH)_{16}\cdot 4H_2O$] and manasseite [$Mg_6Al_2CO_3(OH)_{16}\cdot 4H_2O$]. Ashwal and Cairncross (1997) report an unsuccessful attempt to identify and isolate barbertonite from the type material (housed in the collections of the Harvard Mineralogical Museum). The difficulty involved in isolating and identifying this mineral have led several sources to report barbertonite's status as a mineral to be "questionable" (e.g., Clark 1993). The related mineral, sjögrenite, crystallizes in hexagonal space group $P6_3/mmc$ (No. 194), with a = 3.103 and c = 15.52 Å, which corresponds to the $2H_1$ polytype. Members of the sjögrenite group, which include manasseite and barbertonite,

* E-mail: smills@eos.ubc.ca
† Present address: Department of Geological Sciences, Indiana University, 1001 East 10th Street, Bloomington, Indiana 47405-1405, U.S.A.
‡ Present address: Golder Associates Ltd., 1-25 Scurfield Boulevard, Winnipeg, Manitoba R3Y 1G4, Canada.

are presumed isostructural however, structural data are lacking for manasseite.

Members of the hydrotalcite group[1] have the general formula $A_{6-x}B_{2+x}(OH)_{16}X\cdot 4H_2O$, which is based on positively charged brucite-like layers $(A_{6-x}B_{2+x})(OH)_2$, where A is a divalent cation (e.g., Mg, Fe, Mn, Ni, and Cu) and B is a trivalent cation (e.g., Al, Fe, Cr, Mn, and Ga). Interlayer regions typically contain a monovalent or divalent anion X, such as CO_3^{2-}, SO_4^{2-}, Cl^-, and OH^-. Other anions or a combination of anions may compensate for the positive charge of the brucite-like layers. Water molecules and occasional cations may also be present within the interlayer (Drits et al. 1987; Bookin and Drits 1993). Members of the hydrotalcite group, including stichtite, crystallize in the rhombohedral space group $R\bar{3}m$ (No. 166), with unit-cell parameters $a \approx 3.1$ and $c \approx 23.3$ Å, $V \approx 190$ Å^3, with Z = 3/8 (e.g., Drits et al. 1987). There are currently 13 isostructural natural members of the group, and a large number of synthetic analogues, termed layered double hydroxides (LDHs) or hydrotalcite-like compounds. Several books have been dedicated to this topic (e.g., Rives 2001; Duan and Evans 2006).

The hydrotalcite group is notable for the wide range of polytypism that it exhibits. The nature of this polytypism was discussed by Bookin and Drits (1993) and Bookin et al. (1993a, 1993b), with a more recent summary by Evans and Slade (2006). Polytypism in the hydrotalcite structure-type is complex, but arises due to the different possible ways the brucite-like layer can stack (Bookin and Drits 1993; Evans and Slade 2006). This results in several theoretical polytypes including: one 1-layer (i.e., layer = brucite-like layer and H = hexagonal and R = rhombohedral) polytype ($1H_1$), three 2-layer polytypes ($2H_1$, $2H_2$, $2H_3$), nine 3-layer polytypes ($3R_1$, $3R_2$, $3H_1$–$3H_7$,) and a large number of 6-layer polytypes ($6R$ and $6H$) (Bookin and Drits 1993).

Our interest in stichtite derives from studies of the MKD5 orebody at the Mount Keith Nickel Mine, Western Australia (27°10′S, 120°33′E), where stichtite occurs with other hydrotalcite-like minerals: iowaite [$Mg_6Fe_2Cl_2(OH)_{16}\cdot 4H_2O$], woodallite [$Mg_6Cr_2Cl_2(OH)_{16}\cdot 4H_2O$], hydrotalcite [$Mg_6Al_2CO_3(OH)_{16}\cdot 4H_2O$], pyroaurite [$Mg_6Fe_2CO_3(OH)_{16}\cdot 4H_2O$] and mountkeithite [$(Mg,Ni)_{11}(Fe^{3+},Cr,Al)_3(SO_4,CO_3)_{3.5}(OH)_{24}\cdot 11H_2O$]. Although relatively uncommon in nature, these minerals comprise up to 20 wt% of the serpentinized komatiitic dunite in parts of the orebody at Mount Keith (Grguric 2003; Grguric et al. 2006). Serpentinization and carbonation of the peridotites at Mount Keith resulted from infiltration by low-temperature H_2O-CO_2-rich fluids (Barrett et al. 1977; Grguric et al. 2006). Hydrotalcite-like minerals probably formed by replacement of magnetite and chromite by alkaline fluids during low-grade regional metamorphism (perhaps on the sea floor—E. Melchiorre personal communication). At Mount Keith, early consumption of H_2O and CO_2 resulted in a metasomatic overprint by a Cl-enriched fluid, leading to the high Cl content of the ores, and formation of iowaite- and woodallite-rich ore (Grguric et al. 2006). The interlayer anion sites in hydrotalcite-like minerals preferentially select divalent anions, carbonate in particular (e.g., Bish 1980; Miyata 1983), suggesting that they could be used as mineral traps for anthropogenic and atmospheric CO_2 (Moreira et al. 2006; Woodhouse 2006). Therefore, the high abundance of hydrotalcite-group minerals found at Mount Keith may provide a unique opportunity for both natural and artificially enhanced carbon sequestration.

Here we report the results of Rietveld refinement of the structure of stichtite and the re-examination of the co-type specimens of barbertonite. We discuss the relationship between stichtite and barbertonite and its implication on nomenclature. We also report the Raman spectra of stichtite. Finally, we discuss an application of the crystal structure of stichtite to carbon sequestration.

[1] Hydrotalcite group (and sjögrenite group) are two of several variations used in the literature to group together hydrotalcites. These groupings do not follow the new group standardization hierarchy of Mills et al. (2009), but are used here to maintain continuity.

Experimental methods

Samples

Because hydrotalcite-like minerals at Mount Keith are intergrown with many other phases and tend to have intermediate interlayer compositions, we sought a pure sample of stichtite, from the type locality Stichtite Hill, Tasmania, on which to do detailed structural analyses (University of British Columbia, collection number 1564). Due to the fibrous habit of stichtite and its very low hardness, it is impossible to isolate a single fiber for single-crystal analysis; however, large quantities of stichtite are generally available from the type locality, although they are typically very finely intergrown with serpentine minerals, chlorite-group minerals, various oxides, carbonates, and other phases (Bottrill and Graham 2006). We were, however, able to obtain sufficient pure material for powder diffraction work by carefully removing overgrowths of stichtite from central cores of the relict chromite from which it formed. This was undertaken using fine tweezers under a binocular microscope. In this case we were able to separate stichtite from hand specimens with only extremely minor (<1 wt%) contamination by lizardite.

Two samples of barbertonite, samples 84588 and 92549 housed in the collections of the Harvard Mineralogical Museum are attributed to be the type specimens used by Frondel (1941) in his type description of barbertonite. While documentation does not clearly state if both or one of the samples were used in the initial study, both appear to have been sampled by Frondel. The original X-ray powder film (cf. Fig. 1 in Frondel 1941) has also been retained (with the specimens at Harvard) for both samples. Both samples are rich in "barbertonite," which sits on serpentinite with chromite relics and can be easily sampled without contamination by the host rock.

Powder X-ray diffraction

Samples of stichtite and barbertonite were mounted in 0.5 mm quartz capillaries. The data were collected on a Bruker D8 Advance Cu$K\alpha$ diffractometer with a focusing primary mirror and a VÅNTEC position sensitive detector. Due to the small sample size, an 8 mm Debye slit was used to reduce scattering from the empty capillary. Both conventional and pseudo-variable count-time data sets (Madsen and Hill 1994) were obtained from the sample. Rietveld analyses for structure refinement (Rietveld 1969) were conducted using launch mode within TOPAS V4.2 (Bruker AXS 2008). TOPAS was also used for indexing the data (Table 1). The effect of capillary absorption on the peak intensities was corrected using the correction of Sabine et al. (1998) assuming a capillary packing density of 0.4. The focusing geometry doesn't exhibit peak shifts from capillary absorption, so this was not applied. The mass absorption coefficient of the total capillary contents was used in the absorption correction. Anisotropic peak broadening was fitted using two different techniques. A spherical harmonic relationship (Järvinen 1993) may be applied to the peak widths, which is universally applicable, but requires the addition of many variables to the refinement, depending on the harmonic order used. Instead, the stichtite diffraction pattern was amenable to an alternative approach which uses a reciprocal space relationship with a single variable. This method was previously applied to lithium battery materials with layered structures in the same $R\bar{3}m$ space group (Whitfield et al. 2005a).

Bulk ore from Mount Keith was analyzed using a Siemens D5000 diffractometer at the Department of Earth and Ocean Sciences, University of British Columbia, using Co$K\alpha$ radiation. The sample was prepared according to the methods outlined by Wilson et al. (2006), where 3.00 g of ore and a 0.33 mg of annealed CaF_2 (an internal standard) were ground under anhydrous ethanol with synthetic agate grinding elements for 10 min in a McCrone mill. The homogenized mixture was then loaded into a back-loading aluminum cavity holder of the design described by Raudsepp and Pani (2003) and run under the following conditions: step size

TABLE 1. X-ray powder diffraction data for stichtite and barbertonite (84588)

Stichtite, Stichtite Hill, Tasmania		Barbertonite, Barberton, South Africa	
hkl	d_{obs}	*hkl*	d_{obs}
0 0 3	7.83474(7)	0 0 2	7.81900(3)
0 0 6	3.9174(5)	0 0 4	3.9090(2)
1 0 1	2.66353(3)	0 1 0	2.68100(2)
1 0 4	2.4390(4)	0 1 1	2.64200(3)
0 1 5	2.3287(6)	0 0 6	2.6060(8)
1 0 7	2.095(1)	0 1 2	2.53600(9)
0 1 8	1.980(3)	0 1 3	2.3840(2)
0 0 12	1.959(4)	0 1 4	2.2110(4)
1 0 10	1.767(3)	0 1 5	2.0350(7)
0 1 11	1.671(4)	0 0 8	1.955(2)
0 0 15	1.567(8)	0 1 6	1.869(1)
1 1 0	1.5478(1)	0 1 8	1.579(2)
1 1 3	1.5184(4)	1 1 0	1.5480(1)
1 0 13	1.499(1)	1 1 2	1.5180(2)
1 1 6	1.439(1)	1 1 4	1.4390(6)
0 1 14	1.423(8)	0 1 10	1.351(4)
0 2 1	1.3382(2)	0 2 0	1.3400(2)
2 0 2	1.3318(2)	1 1 6	1.331(2)
1 1 9	1.331(3)	0 2 2	1.3210(2)
0 2 4	1.3068(7)	0 2 3	1.2980(4)
0 0 18	1.31(1)	0 2 4	1.2680(7)
2 0 5	1.289(1)	0 2 6	1.192(2)
1 0 16	1.29(1)	0 0 14	1.12(1)
0 2 7	1.245(2)	0 2 8	1.106(3)
0 1 17	1.23(1)	1 1 10	1.100(5)
2 0 8	1.219(3)	2 1 0	1.0130(4)
1 1 12	1.214(7)	2 1 2	1.0050(4)
0 2 10	1.164(5)	2 1 3	0.9950(6)
2 0 11	1.135(6)	2 1 4	0.981(1)
1 0 19	1.12(1)	0 0 16	0.98(1)
0 0 21	1.12(2)	0 2 11	0.975(7)
0 2 13	1.077(9)	0 1 15	0.97(1)
0 1 20	1.08(2)		
2 0 14	1.05(1)		
2 1 1	1.0123(4)		
1 2 2	1.0095(4)		
2 1 4	0.999(1)		
1 1 18	0.99(2)		
1 0 22	0.99(3)		
1 2 5	0.991(1)		
0 2 16	0.99(1)		
0 0 24	0.98(3)		
2 1 7	0.970(3)		
2 0 17	0.96(1)		

0.04 °2θ and counting time of 0.8 s/step over a range of 3–80 °2θ. Quantitative phase analysis was undertaken with TOPAS V3 (Bruker AXS 2004) using the fundamental parameters approach (Cheary and Coelho 1992). The method of Wilson et al. (2006) was used to compensate for structural disorder in lizardite and antigorite during refinement.

Raman spectroscopy

Near-infrared Raman analysis was performed on a sample of Tasmanian stichtite using a Renishaw Imaging Microscope System 1000 (Department of Biochemistry, UBC), with a RL785 diode laser at a wavelength of 785 nm, a RenCam CCD detector and Renishaw WiRE Version 1.3.30 instrument control software. The data were analyzed using Galatic Grams/32 Version 4.14 software. Prior to data acquisition, a spectral calibration was carried out using the Raman spectrum obtained from a silicon wafer. Spectra were recorded in backscatter mode between 150 and 3000 cm^{-1} with a spectral resolution of ±2 cm^{-1} and a minimum lateral resolution of ~5 by 3 µm on the sample. We were unable to obtain any information above 3000 cm^{-1}.

SAMPLE DESCRIPTION AND STRUCTURE

Stichtite, Tasmania, Australia

A Rietveld refinement plot for the stichtite sample from Tasmania is shown in Figure 1. The X-ray powder diffraction (XRPD) pattern is dominated by the reflections of the rhombohedral hydrotalcite-group polytype, $3R_1$, with space group $R\bar{3}m$. However, less intense peaks are also noted corresponding to the $2H_1$ polytype, as well as peaks corresponding to lizardite. It is commonplace in the literature to consider individual reflections such as 003 and 006 when identifying the various polytypes, in addition to calculating the oxygen content of the interlayer site (e.g., Kloprogge et al. 2002; Thomas et al. 2004). In this study, we employ full-pattern fitting with the Rietveld method to determine the crystal structure of stichtite.

The first two stichtite reflections 003 and 006 completely dominate the pattern, even when using a square root intensity scale (as shown in Fig. 1). Without additional constraints, these reflections will completely dominate the least-squares fitting process, even with properly scaled variable count data. To reduce bias in the fitting process, and to better access the information available at high angles, the intensity data below 30 °2θ were scaled to 10% of their initial values. By scaling the low-angle intensity data, misfits in that region will not dominate the refinement; however, one side effect of this weighting scheme is that the R_{wp} residual will be slightly larger than it would be otherwise.

The high symmetry of the $3R_1$ polytype suggests that Rietveld fitting and refinement should be routine; however, since the hydrotalcite structure contains mixed and partially occupied anion sites, this makes an unconstrained refinement using a single set of XRPD data theoretically impossible. A suitable analogy would be a set of simultaneous equations with 3 or more variables with insufficient information available to solve them. Extra information with differing atomic contrasts may be supplied using neutron diffraction and/or resonant diffraction (Whitfield et al. 2005b), but a single data set requires significant constraints to prevent over-parameterization. The traditional description of the compositions of hydrotalcite-like minerals does not follow neatly from the multiplicities in the $R\bar{3}m$ unit cell. A factor of 8/3 must be applied to all the calculations of occupancies, explained by the placing of nominally 8 cations ($6 \times$ Mg plus $2 \times$ Cr) on a site with threefold multiplicity.

The proposed structural model involves placement of the atoms on the following sites in $R\bar{3}m$:

3*a*	(0,0,0)	Mg^{2+}, Cr^{3+}
6*c*	(0,0,*z*)	O, H (hydroxide)
6*c*	(1/3,2/3,1/2)	C (carbonate)
18*h*	(*x*,–*x*,1/2)	O (water + carbonate)

Assuming that the cation and hydroxide sites are fully occupied makes the application of compositional constraints on the anion occupancies feasible. That leaves the additional scattering from the water O atoms the only freely refined occupancy variable. Details of the structure refinement strategy employed are given by Whitfield et al. (2010). There have been few previous Rietveld refinements of similar materials, and these have mostly been conducted on Cl^--dominant synthetic hydrotalcites (e.g., Ennadi et al. 2000; Roussel et al. 2000; Simon et al. 2003), while Bellotto et al. (1996) reported Rietveld analyses for synthetic hydrotalcite, but did not refine the positions of the OH and CO_3 and considered them "incorrect."

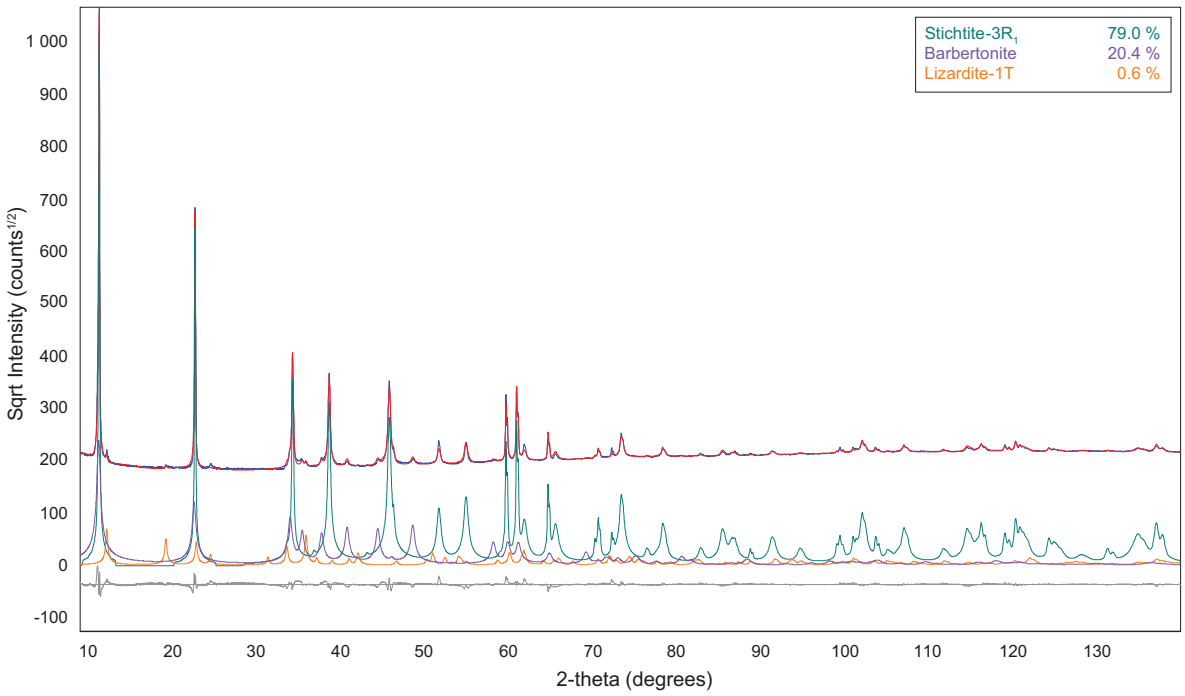

FIGURE 1. Difference plot from the Rietveld refinement of the stichtite data from Tasmania (using Cu$K\alpha$ radiation). Uppermost lines = observed data overlain by calculated pattern; gray line below = residual pattern; curves under the observed and calculated patterns = calculated patterns of each phase. Axes are square root of the intensity (counts) vs. 2θ (degrees).

TABLE 2. Atomic coordinates and displacement parameters (Å²) for stichtite and barbertonite

Sample	Tasmania, Australia Stichtite	84588; Barberton, South Africa Barbertonite	92459; Barberton, South Africa Barbertonite
a	3.095518(31)	3.09689(6)	3.09646(6)
c	23.50421(67)	15.6193(8)	15.627(1)
V	195.0486(68)	129.731(8)	129.76(1)
sof (Mg/Cr)*	0.77(2):0.23(2)	0.75(2):0.25(2)	0.81(2):0.19(2)
B_{iso} (Mg/Cr)*	0.16(6)	0.8(1)	1.62(12)
z (O1)†	0.37268(6)	0.0650(3)	0.0589(4)
B_{iso} (O1)†	0.04(1)	0.64(15)	1.7(2)
z (H1)‡	0.41108(53)	0.131(5)	–0.007(7)
B_{iso} (H1)‡	0.04(1)	0.64(15)	1.7(2)
x (O2)§	0.1242(7)	0.23(63)	0.23(41)
–*x* (O2)§	0.8758(7)	–0.23(63)	–0.23(41)
sof (O2)§	0.161(6)	0.155(6)	0.130(7)
B_{iso} (O2)§	0.02(2)	0.64(15)	1.7(2)
sof (C1)‖	0.059(5)	0.124(8)	0.097(9)
B_{iso} (C1)‖	0.02(2)	0.64(15)	1.7(2)
R_p (%)	1.62	2.12	1.89
R_{wp} (%)	2.01	3.44	2.53
GOF	3.74	4.22	3.11

Note: H2 fixed at *sof* = 0.5.
* Mg on (0,0,0).
† O1 on (1/3,2/3,*z*).
‡ H1 on (1/3,2/3,*z*).
§ O2 on (*x*,–*x*,1/4) for barbertonite or (*x*,–*x*,1/2) for stichtite.
‖ C1 on (0,0,1/4) for barbertonite or (1/3,2/3,1/2) for stichtite.

TABLE 3. Polyhedral bond distances (Å) in stichtite and barbertonite

Sample	Tasmania, Australia Stichtite	84588; Barberton, South Africa Barbertonite	92459; Barberton, South Africa Barbertonite
Mg/Cr-O1	2.0123(8)	2.056(3)	2.011(3)
O1-O1	2.572(2)	2.706(8)	2.566(9)
O1-O2	3.065(2)	2.94(5)	3.04(30)
C1-O2	1.121(4); 1.5644(6)	1.20(24)	1.20(16)

The refined coordinates for stichtite-3R_1 are shown in Table 2 and interatomic bond lengths in Table 3. The final refined composition for the stichtite-3R_1 is $Mg_{6.12}Cr_{1.88}(OH)_{16}(CO_3)_{0.94}\cdot 4.9H_2O$, which is consistent with a hydrotalcite-group member and close to the ideal formula. The large interlayer space in which the water molecule resides can accommodate more than 4 molecules per formula unit. Synthetic hydrotalcite-like compounds have been shown to have greatly varying water contents, depending not only on the cations involved in the synthesis, but also the anions situated in the interlayer (e.g., Miyata 1980; Radha and Kamath 2009). In synthetic CO_3-bearing hydrotalcite-like compounds, water contents can vary by ~10 wt%, which may reflect subtle changes in temperature and formation conditions (e.g., Miyata 1980). The bond lengths in stichtite-3R_1 are fairly typical of those found in hydrotalcites: Mg/Cr-O1 is 2.0123(8) Å, the hydrogen bond to O1 is 0.9 Å; the mixed carbonate-hydrogen site has bonds of 1.121(4) and 1.5644(6) Å to the corresponding O2 atom. The Mg/Cr octahedron is flattened and distorted, but matches closely with that reported for Mg/Al hydrotalcite (e.g., Allmann and Jepsen 1969; Bellotto et al. 1996). The C-O bonds in stichtite are atypical due to incorporation of hydroxyl on the same site. This results in the carbonate being strongly distorted away from typical equilateral triangular geometry such as that observed in calcite (where the C-O is ~1.28 Å). However, the refined positions are consistent with the unrefined model of Bellotto et al. (1996), indicating that this feature is typical for hydrotalcite minerals and its synthetic equivalents.

Rietveld refinement of the Tasmanian sample (Fig. 1) shows 79.2 wt% is comprised of stichtite-3R_1, 0.6 wt% lizardite-1*T* and

the remainder (20.2 wt%) is the $2H_1$ polytype (=barbertonite). After the successful modeling of the rhombohedral stichtite, a model for the hexagonal polytype could be derived by the same methods as above, where the Mg/Cr ion is sited on (0, 0, 0), O1 and H1 on (1/3, 2/3, *z*), O2 on (*x*, –*x*, 1/4), and the mixed carbonate-hydrogen site on (0, 0, 1/4). This model was tested on the samples from Barberton (see below). The refined coordinates for stichtite-$2H_1$ are shown in Table 2 and interatomic bond lengths in Table 3. A view of the structures along **a** is shown in Figure 2. The composition for the stichtite-$2H_1$ was fixed to be equal to that of the stichtite-$3R_1$, because the low abundance and the nature of interlayer site precluded refinement.

Barbertonite, Barberton, South Africa

Because previous studies failed to verify the presence of barbertonite in the type specimens (e.g., Ashwal and Cairncross 1997), both were re-examined in this study (Fig. 3). Upon examination of the type specimens, the exact sampling spot of Frondel (1941) could be observed, where a large vertical scratch mark was prominent on the surface of the specimen. Material used in this study was extracted adjacent to these scratch marks to match as closely as possible the material studied by Frondel (1941). Rietveld refinement of XRPD data from the two samples shows a mixture of the $3R_1$ and the $2H_1$ polytypes. Notably, these samples contain a greater proportion of the $2H_1$ polytype than was observed in the Tasmanian sample. Specimen 92549 contains 54.4 wt% stichtite-$3R_1$ and 45.6 wt% barbertonite, while specimen 84588 contains 46.5 wt% stichtite-$3R_1$ and 53.5 wt% barbertonite (Fig. 4). The higher proportion of barbertonite in these samples enabled all parameters for both species to be refined. The refined coordinates are shown in Table 2 and interatomic bond lengths are given in Table 3. CIF[2] material on deposit.

The cell dimensions and bond lengths for barbertonite in both of the co-type samples are practically identical. Likewise, the refinement of the coexisting stichtite gave almost identical unit-cell dimensions and bond lengths. Minor variations in bond lengths are primarily due to a change in the Mg:Cr ratio. The refinements suggest that the Mg:Cr ratio may in fact be slightly larger in barbertonite than that observed in stichtite; however, the differences between them are unlikely to aid in distinguishing the two species chemically. In fact, the *a* cell dimension is virtually identical for both stichtite and barbertonite from Tasmania and Barberton. The only definitive way of separating the two species is a close inspection of the PXRD patterns in the region 30–50° 2θ (Fig. 4), where separation of the peaks is easily observed. Mismatches in the intensities of the 003 and 006 reflections may also aid in the distinction between stichtite and barbertonite.

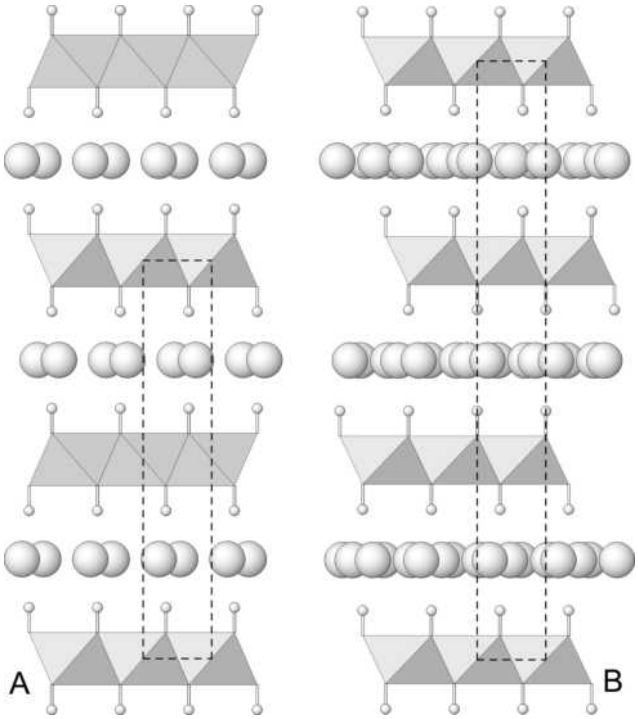

FIGURE 2. Crystal structures of (**a**) barbertonite ($2H_1$) and (**b**) stichtite ($3R_1$) projected along **a**. Unit cells are shown by dashed lines.

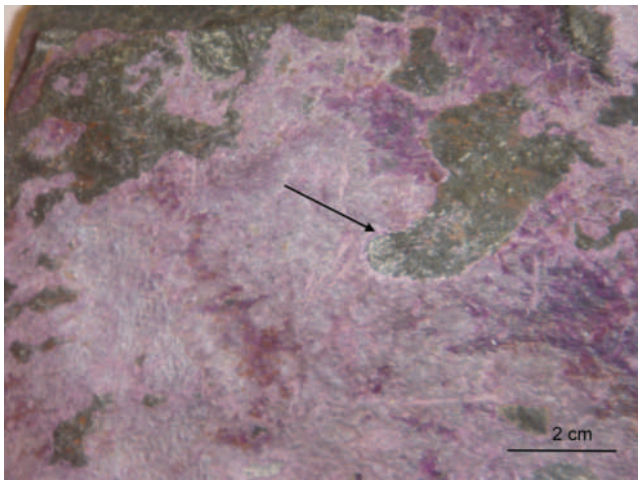

FIGURE 3. Co-type specimen 84588 of barbertonite from Barberton, South Africa. Sampling area of Frondel and this study indicated by arrow. Field of view approximately 10 cm.

Raman analyses

Raman analyses of the stichtite sample shows several major bands. Two *M*-OH stretching bands are observed at 2632 and 2621 cm^{-1}, which can be attributed to MgOH and CrOH vibrations. These bands have been observed rarely (e.g., Lin et al. 2003) and may serve as one diagnostic for stichtite identification. Interestingly, mountkeithite $(Mg,Ni)_{11}(Fe^{3+},Cr,Al)_3(SO_4,CO_3)_{3.5}(OH)_{24}\cdot 11H_2O$, also exhibits these bands (Lin et al. 2003). The structure of mountkeithite however, appears to be different from that of hydrotalcite (Hudson and Bussell 1981). No bands are observed in the H_2O bending region for stichtite. All of the modes for the carbonate ion are Raman-active in stichtite. This is different from the results of Frost and Erikson (2004) who reported that only the ν_1 symmetric stretching mode was Raman-active in

[2] Deposit item AM-11-013, CIFs. Deposit items are available two ways: For a paper copy contact the Business Office of the Mineralogical Society of America (see inside front cover of recent issue) for price information. For an electronic copy visit the MSA web site at http://www.minsocam.org, go to the *American Mineralogist* Contents, find the table of contents for the specific volume/issue wanted, and then click on the deposit link there.

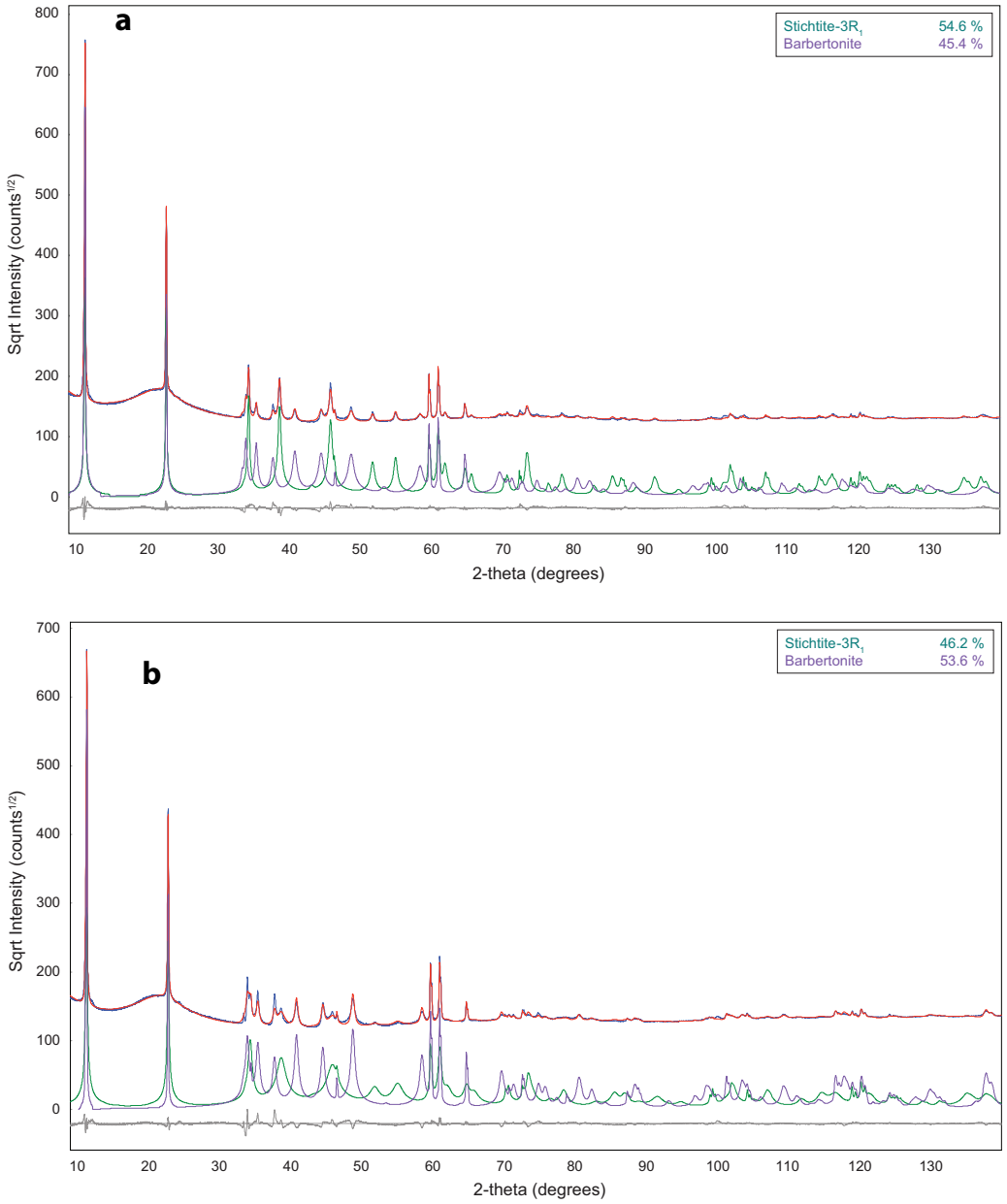

FIGURE 4. Difference plot from the Rietveld refinement of the barbertonite data from Barberton (using Cu$K\alpha$ radiation). Specimen 92549 (**a**) and 84588 (**b**). Uppermost lines = observed data overlain by calculated pattern; gray line below = residual pattern; curves under the observed and calculated patterns = calculated patterns of each phase. Axes are square root of the intensity (counts) vs. 2θ (degrees).

synthetic stichtite. The ν_3 asymmetric stretching mode, which is absent in some hydrotalcite species, is present at 1343 cm^{-1} and shifted to much lower wavenumbers than expected [~1400 cm^{-1} in Kloprogge et al. (2002)]. When present, ν_3 appears to have greater intensity in the hexagonal polytypes [e.g., manasseite; Frost and Reddy (2006)] than in the trigonal [e.g., hydrotalcite; Kloprogge et al. (2002)]. The shift from ~1400 cm^{-1} appears to be primarily due to the atypical coordination described above. It is, therefore, possible that the prevalence of ν_3 in the stichtite spectra could be a result of barbertonite admixture. Due to the nature of their intergrowth, it is impossible to categorically confirm or deny this. Chemical tests (by the CHN method) indicated no nitrate present in the sample.

The ν_1 symmetric stretching mode of the carbonate is centered at 1055 cm^{-1} and is asymmetric, indicating the presence of one or more extra peaks. This strongly suggests that D_{3h} symmetry is not maintained and instead that the site symmetry has been lowered to C_{2v} or C_s. These results are consistent with that reported by Kloprogge and Frost (1999). The ν_2 stretching mode of the carbonate is extremely weak and present at 860 cm^{-1}. This band is not Raman-active when D_{3h} symmetry is maintained, further suggesting C_{2v} or C_s symmetry. Two bands are present at 685 and 672 cm^{-1} and can be attributed to the E_g(T) mode of (Mg/Cr)-OH (e.g., Kagunya et al. 1998) and the ν_4 stretching mode of the carbonate, respectively. The ν_2 bending mode of the carbonate is present at 534 cm^{-1}. The only other observable band is located at 428 cm^{-1} and is most likely due to a lattice mode involving of Mg and/or Cr.

IMPLICATIONS FOR CARBON SEQUESTRATION

Finely ground mine tailings can be highly reactive at low temperature and are, therefore, of interest as a sink or potential source of greenhouse gases. Wilson et al. (2009) have shown that mine tailings can absorb CO_2 from the atmosphere, thereby

offsetting some of the greenhouse gas emissions associated with mining activities. The nature of the host species that bind carbon crystallographically was critical for assessing the amount of stored CO_2 in that study, since gangue minerals (e.g., magnesite) and surface precipitates (e.g., hydromagnesite) play different roles and must be distinguished. Hydrotalcite group minerals provide another important potential reservoir of CO_2, because they readily exchange carbonate for other anions in low-temperature environments such as mineral processing facilities (Grguric et al. 2006).

Rietveld refinement of XRPD data from a sample of Mount Keith ore (Fig. 5) show that hydrotalcite-like minerals make up a large proportion of the sample. In this case, 6.1 wt% of the sample comprises stichtite-3R_1 and 5.6 wt% iowaite. End-member stichtite contains 6.73% CO_2 by mass. If sample 06MKOre is representative of the roughly eleven million metric tons of ore processed at the Mount Keith Nickel mine annually, then the amount of CO_2 mined as stichtite at Mount Keith could exceed 45 000 metric tons per year. Exchange of CO_2 for Cl or SO_4 at surface conditions represents a greenhouse gas release hazard. Conversely, the exchange of Cl for CO_3 could fix in excess of 40 000 metric tons CO_2 per year, if end-member iowaite is reacted to form pyaroaurite. Total greenhouse gas emissions at Mount Keith are approximately 350 000 metric tons CO_2 equivalent (Wilson et al. 2009). Careful stewardship of anion exchange reactions in hydrotalcite group minerals could, thus, substantially impact the greenhouse gas emissions of mine operations.

Implications for nomenclature

Rietveld refinements of both stichtite and barbertonite show that they are polytypes of one another (Fig. 2). According to Nickel and Grice (1998) "Polytypes and polytypoids are not regarded as separate species and, like topologically similar polymorphs, they can be distinguished by the addition of a crystallographic suffix to the mineral name." Therefore, because stichtite has historical priority (1914) over barbertonite (1941), these polytypes should be denoted as stichtite-3*R* and stichtite-2*H* (=barbertonite). Additionally, Tatarinov et al. (1985) and Bookin et al. (1993b) reported the presence of stichtite-1*H* admixed with stichtite-3*R* from the Terektinsky Ridge, Altai Mountains, Altai Republic, Russian Federation. Some Tasmanian samples previously labeled as barbertonite were found by PXRD to be mostly stichtite with only minor barbertonite, although the polytypes were not defined (Bottrill and Graham 2006).

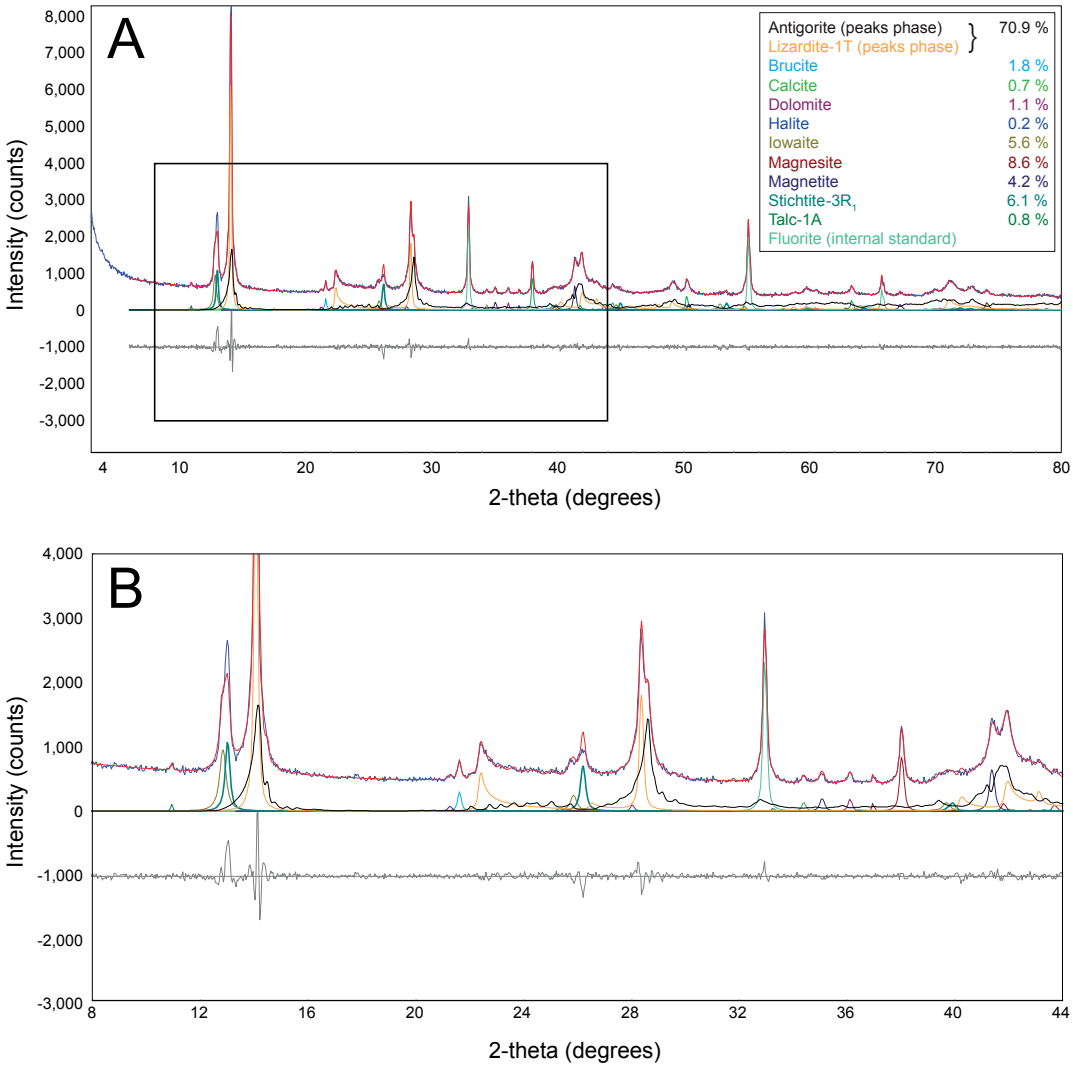

Figure 5. Rietveld refinement plot of a representative sample of Mount Keith ore; (**a**) full pattern, (**b**) boxed region where hydrotalcite strong reflections are present (using Co*K*α radiation). Uppermost lines = observed data overlain by calculated pattern; gray line below = residual pattern; curves under the observed and calculated patterns = calculated patterns of each phase. Axes are intensity (counts) vs. 2θ (degrees).

Other possibilities have been suggested for the nomenclature of the hydrotalcite and sjögrenite groups. Drits et al. (1987), for example, suggested that a single root name should be given based on the composition of the brucite-like layers, along with information on the polytype, repeat distance and dominant ion in the interlayer. Using this scheme, manasseite would become 7.56 Å CO_3-hydrotalcite-2*H* (Drits et al. 1987). While this name is rich in information about the mineral, it is not ideal for classification and would be anomalous in mineralogical nomenclature. It also does not take the structural ordering found in some members [e.g., quintinite, $Mg_4Al_2CO_3(OH)_{12}\cdot H_2O$—Arakcheeva et al. (1996); Chao and Gault (1997)] into account. Another possibility could be the use of suffixes to denote the different compositions within the group.

It seems reasonable to apply a naming scheme based on historical priority to other existing members of the hydrotalcite and sjögrenite groups that are polytypes, e.g., manasseite (=hydrotalcite-2*H*). However, we recognize that the general application of polytype suffixes to appropriate members of these groups and the accompanying discreditation of certain species, is beyond the scope of this work, and requires a broader study under the auspices of the Commission on New Minerals, Nomenclature and Classification (CNMNC) of the International Mineralogical Association (IMA). At this time, group nomenclature may also be revisited, whereby various group names commonly in use for the various minerals will be streamlined in accordance with the IMA-CNMNC approved group nomenclature of Mills et al. (2009).

Acknowledgments

We thank Editor Martin Kunz, Associate Editor Ian Swainson, and referees Andrew Christy, Anthony Kampf, and Ralph Bottrill who provided helpful comments on the manuscript. We acknowledge the support of the Natural Sciences and Engineering Research Council of Canada (Discovery Grants to M.R. and G.M.D.). Work by S.A.W. was supported by an Alexander Graham Bell Canada Graduate Scholarship from the Natural Sciences and Engineering Research Council of Canada. Marcia Yu and Kadek Okuda (Department of Biochemistry, UBC) are thanked for providing access to the Raman microscope and Anton Beran (University of Vienna) is thanked for advice on Raman spectra. This is publication 199 of the Mineral Deposit Research Unit.

References cited

Allmann, R. and Jepsen, H.P. (1969) Die Struktur des Hydrotalkits. Neues Jahrbuch für Mineralogie Monatshefte, 544–551 (in German with English abstract).

Arakcheeva, A.V., Pushcharovsky, D.Y., Rastsvetaeva, R.K., Atencio, D., and Lubman, G.U. (1996) Crystal structure and comparative crystal chemistry of $Al_2Mg_4(OH)_{12}(CO_3)\cdot 3H_2O$, a new mineral from the hydrotalcite-manasseite group. Crystallography Reports, 41, 972–981.

Ashwal, L.D. and Cairncross, B. (1997) Mineralogy and origin of stichtite in chromite-bearing serpentinites. Contributions to Mineralogy and Petrology, 127, 75–86.

Barrett, F.M., Binns, R.A., Groves, D.I., Marston, F.J., and McQueen, K.G. (1977) Structural history and metamorphic modification of Archean volcanic-type nickel deposits, Yilgarn Block, Western Australia. Economic Geology, 77, 1195–1223.

Bellotto, M., Rebours, B., Clause, O., and Lynch, J. (1996) A reexamination of hydrotalcite crystal chemistry. Journal of Physcial Chemistry, 100, 8527–8534.

Bish, D.L. (1980) Anion-exchange in takovite: applications to other hydroxide minerals. Bulletin of Mineralogy, 103, 170–175.

Bookin, A.S. and Drits, V.A. (1993) Polytype diversity of the hydrotalcite-like minerals. I. Possible polytypes and their diffraction features. Clays and Clay Minerals, 41, 551–557.

Bookin, A.S., Cherkashin, V.I., and Drits, V.A. (1993a) Polytype diversity of the hydrotalcite-like minerals. II. Determination of the polytypes of experimentally studied varieties. Clays and Clay Minerals, 41, 558–564.

——— (1993b) Reinterpretation of the X-ray diffraction patterns of stichtite and reevesite. Clays and Clay Minerals, 41, 631–634.

Bottrill, R.S. and Graham, I.T. (2006) Stichtite from Western Tasmania. Australian Journal of Mineralogy, 12, 101–107.

Chao, G.Y. and Gault, R.A. (1997) Quintinite-2H, quintinite-3T, charmarite-2H, charmarite-3T and caresite-3T, a new group of carbonate minerals related to the hydrotalcite-manasseite group. Canadian Mineralogist, 35, 1541–1549.

Cheary, R.W. and Coelho, A.A. (1992) A fundamental parameters approach to X-ray line-profile fitting. Journal of Applied Crystallography, 25, 109–121.

Clark, A.M. (1993) Hey's Mineral Index, 3rd ed. Chapman and Hall, London.

Drits, V.A., Sokolova, T.N., Sokolova, G.V., and Cherkashin, V.I. (1987) New members of the hydrotalcite-manasseite group. Clays and Clay Minerals, 35, 401–417.

Duan, X. and Evans, D.G. (2006) Layered double hydroxides. Springer, Berlin, 218 pp.

Ennadi, A., Legrouri, A., de Roy, A., and Besse, J.P. (2000) X-Ray diffraction pattern simulation for thermally treated [Zn-Al-Cl] layered double hydroxide. Journal of Solid State Chemistry, 152, 568–572.

Evans, D.G. and Slade, R.C.T. (2006) Structural aspects of layered double hydroxides. Structure and Bonding, 119, 1–87.

Frost, R.L. and Erikson, K.L. (2004) Vibrational spectroscopy of stichtite. Spectrochimica Acta Part A, 60, 3001–3005.

Frost, R.L. and Reddy, B.J. (2006) Thermo-Raman spectroscopic study of the natural layered double hydroxide manasseite. Spectrochimica Acta Part A, 65, 553–559.

Frondel, C. (1941) Constitution and polymorphism of the pyroaurite and sjögrenite groups. American Mineralogist, 26, 295–315.

Grguric, B.A. (2003) Minerals of the MKD5 nickel deposit, Mount Keith, Western Australia. Australian Journal of Mineralogy, 9, 55–71.

Grguric, B.A., Rosengren, N.M., Fletcher, C.M., and Hronsky, J.M.A. (2006) Type 2 deposits: geology, mineralogy and processing of the Mount Keith and Yakabindi orebodies, Western Australia. Society of Economic Geologists Special Publications, 13, 119–138.

Hudson, D.R. and Bussell, M. (1981) Mountkeithite, a new pyroaurite-related mineral with an expanded interlayer containing exchangeable $MgSO_4$. Mineralogical Magazine, 44, 345–350.

Järvinen, M. (1993) Application of symmetrized harmonics expansion to correction of the preferred orientation effect. Journal of Applied Crystallography, 26, 525–531.

Kagunya, W., Baddour-Hadjean, R., Kooli, F., and Jones, W. (1998) Vibrational modes in Layered Double Hydroxides and their calcined derivatives. Chemical Physics, 236, 225–234.

Kloprogge, J.T. and Frost, R.L. (1999) Fourier transform infrared and Raman spectroscopic study of the local structure of Mg, Ni and Co hydrotalcites. Journal of Solid State Chemistry, 146, 506–515.

Kloprogge, J.T., Wharton, D., Hickey, L., and Frost, R.L. (2002) Infrared and Raman study of the interlayer anions CO_3^{2-}, NO_3^-, SO_4^{2-}, and ClO_4^- in Mg/Al hydrotalcite. American Mineralogist, 87, 623–629.

Lapham, D.M. (1958) Structural and chemical variation in chromium chlorite. American Mineralogist, 43, 921–956

Lin, Y.-H., Adebajo, M.O., Kloprogge, J.T., Martens, W.N., and Frost, R.L. (2003) X-ray diffraction and Raman spectroscopic studies of Zn-substituted carrboydite-like compounds. Materials Chemistry and Physics, 100, 174–186.

Madsen, I.C. and Hill, R.J. (1994) Collection and analysis of powder diffraction data with near-constant counting-statistics. Journal of Applied Crystallography, 27, 385–392.

Mills, S.J., Hatert, F., Nickel, E.H., and Ferraris, G. (2009) The standardisation of mineral group hierarchies: application to recent nomenclature proposals. European Journal of Mineralogy, 21, 1073–1080.

Miyata, S. (1980) Physico-chemical properties of synthetic hydrotalcites in relation to composition. Clays and Clay Minerals, 28, 50–56.

——— (1983) Anion-exchange properties of hydrotalcite-like compounds. Clays and Clay Minerals, 31, 305–311.

Mondal, S.K. and Baidya, T.K. (1996) Stichtite $[Mg_6Cr_2(OH)_{16}CO_3\cdot 4H_2O]$ in the Nuasahi ultramafites, Orissa, India—its transformation at elevated temperatures. Mineralogical Magazine, 60, 836–840.

Moreira, R.F.P.M., Soares, J.L., Casarin, G.L., and Rodrigues, A.E. (2006) Adsorption of CO_2 on hydrotalcite-like compounds in a fixed bed. Separation Science and Technology, 41, 341–357.

Nickel, E.H. and Grice, J.D. (1998) The IMA Commission on New Minerals and Mineral Names: procedures and guidelines on mineral nomenclature. Canadian Mineralogist, 36, 913–926.

Nordenskiöld, N. (1840) Description of kammererite, a new mineral from Siberia. Acta Societas Scientiarum Fennica, 1, 483–487 (in Swedish).

Petterd, W.F. (1910) Catalog of the minerals of Tasmania. Mines Department Publication, John Vail Printers, Government Printer, Hobart, 167–169.

Radha, S. and Kamath, P.V. (2009) Polytype selection and structural disorder mediated by intercalated sulfate ions among the layered double hydroxides of Zn with Al and Cr. Crystal Growth and Design, 9, 3197–3203.

Raudsepp, M. and Pani, E. (2003) Application of Rietveld analysis to environmental mineralogy. In J.L. Jambor, D.W. Blowes, and A.I.M. Ritchie, Eds. Environmental mineralogy of mine wastes. Mineralogical Association of Canada Short Course, 31, 165–180.

Rietveld, H.M. (1969) A profile refinement method for nuclear and magnetic structures. Journal of Applied Crystallography, 2, 65–71.

Rives, V. (2001) Layered double hydroxides: present and future. Nova Science Publishers, Huntington, 439 pp.

Roussel, H., Briois, V., Elkaim, E., de Roy, A., and Besse, J.P. (2000) Cationic order and structure of [Zn-Cr-Cl] and [Cu-Cr-Cl] layered double hydroxides: A XRD and EXAFS study. Journal of Physical Chemistry B, 104, 5915–5923.

Sabine, T.M., Hunter, B.A., Sabine, W.R., and Ball, C.J. (1998) Analytical expressions for the transmission factor and peak shift in absorbing cylindrical specimens. Journal of Applied Crystallography, 31, 47–51.

Simon, L., François, M., Refait, P., Renaudin, G., Lelaurain, M., and Génin, J.-M.R. (2003) Structure of the Fe(II-III) layered double hydroxysulphate green rust two from Rietveld analysis. Solid State Sciences, 5, 327–334.

Tatarinov, A.V., Sapozhnikov, A.N., Prokudin, S., and Frolova, L.P. (1985) Stichtite in serpentinites of the Terektinsky Ridge (Gornyi Altai). Zapiski Vsesoyuznogo Mineralogicheskogo Obshchestva, 114, 575–581 (in Russian).

Thomas, G.S., Rajamathi, M., and Kamath, P.V. (2004) DIFFaX simulations of polytypism and disorder in hydrotalcite. Clays and Clay Minerals, 52, 693–699.

Twelvetrees, W.H. (1914) Stichtite. A new Tasmanian mineral. Notes by various authors, collected and edited. Tasmania Department of Mines, Geological Survey Record No 2.

Whitfield, P.S., Niketic, S., Le Page, Y., and Davidson, I.J. (2005a) Investigating the nature of anisotropic line broadening in electrochemically delithiated $Li_{1.2}Mn_{0.4}Ni_{0.3}Co_{0.1}O_2$. Advances in X-ray Analysis, 49, 149–155.

Whitfield, P.S., Davidson, I.J., Cranswick, L.M.D., Swainson, I.P., and Stephens, P.W. (2005b) Investigation of possible superstructure and cation disorder in the lithium battery cathode material $LiMn_{1/3}Ni_{1/3}Co_{1/3}O_2$ using neutron and anomalous dispersion powder diffraction. Solid State Ionics, 176, 463–471.

Whitfield, P.S., Davidson, I.J., Mitchell, L.D., Wilson, S.A., and Mills, S.J. (2010) Problem solving with the TOPAS macro language: Corrections and constraints in simulated annealing and Rietveld refinement. Materials Science Forum, 651, 11–25.

Wilson, S.A., Raudsepp, M., and Dipple, G.M. (2006) Verifying and quantifying carbon mine tailings using the Rietveld method with X-ray powder diffraction data. American Mineralogist, 91, 1331–1341.

Wilson, S.A., Dipple, G.M., Power, I.M., Thom, J.M., Anderson, R.G., Raudsepp, M., Gabites, J.E., and Southam, G. (2009) Carbon dioxide fixation within mine wastes of ultramafic-hosted ore deposits: Examples from the Clinton Creek and Cassiar chrysotile deposits, Canada. Economic Geology, 104, 95–112.

Woodhouse, J.N. (2006) The characterization of hydrotalcite-group minerals and their anion exchange capabilities at Mount Keith Nickel Mine, Western Australia. B.Sc. Thesis, The University of British Columbia, Vancouver, British Columbia.

Manuscript received February 3, 2010
Manuscript accepted August 11, 2010
Manuscript handled by Ian Swainson